ACS OMEGA

Article

http://pubs.acs.org/journal/acsodf

In Situ Growth of Low-Dimensional Silver Nanoclusters with Their Tunable Plasmonic and Thermodynamic Behavior

Gajendra Kumar Inwati,[†] Yashvant Rao,[†] and Man Singh*[,‡]

[†]Centre for Nanosciences and [‡]School of Chemical Sciences, Central University of Gujarat, Sector-30, Gandhinagar 382030, India

Supporting Information

ABSTRACT: Optical properties of noble metal nanostructures associated with localized surface plasmon resonance (SPR) are technically important for optical switches and plasmonic devices. In this work, silver nanoclusters are embedded inside the soda-lime glass matrix, followed by a thermal annealing process in an open air atmosphere for 1 h. The effects of thermal annealing on the plasmonic behavior of Ag nanoclusters embedded in the glass matrix are studied with UV−vis spectroscopy and photoluminescence. In the SPR spectra, a 14 nm blue shift is observed in the visible range under the influence of thermal annealing at a higher temperature. The thermal effects on Ag particle size and SPR have been illustrated for plasmonic properties. The structural and elemental investigation of as-grown Ag nanoclusters is confirmed by X-ray diffraction, high-resolution transmission electron microscope, and X-ray photoelectron spectroscopy. The structural, plasmonic, and thermodynamic properties associated with the growth mechanism of Ag nanoclusters have been explained under the thermal process. Enthalpy (ΔH), entropy (ΔS), and Gibbs energy (ΔG) for Ag nanoclusters growth and nucleation are significantly calculated and interpreted at different temperatures. An empirical relation among the ΔH, ΔS, and ΔG is developed vis-a-vis activation energy (97.70 J/mol), which is calculated by the Arrhenius linear equation.

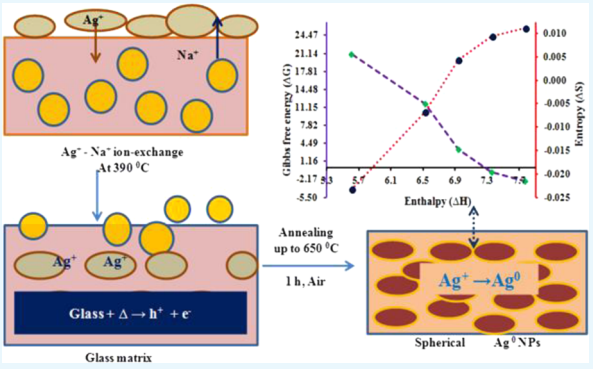

1. INTRODUCTION

Over the past few decades, plasmon-based noble metallic nanostructures, such as Ag, Au, and Cu, under the category of transitional metals, have drawn tremendous scientific attention and interest due to their tunable plasmonic and catalytic behavior on the nanoscale. Such embedded metallic nanostructures are significantly used in various applications, such as optoelectronics,[1−3] catalysis,[4] detection,[5] and biomedicine.[6] In the field of plasmons, the noble metal nanoclusters, which are dispersed in a transparent glass matrix, exhibit both linear and nonlinear optical surface plasmon resonance (SPR) properties. These nanostructures are highly useful for surface-plasmon-based applications, like surface-enhanced fluorescence,[7] surface-enhanced Raman scattering,[8] and nanophotonic devices and circuits.[9] The interaction of electromagnetic radiation with such a metal-nanocluster-embedded glass matrix exhibits characteristic SPR in the visible region due to a coherent oscillation of conduction band electrons.[10] Thus, the resonance frequency of metallic nanoclusters could be tuned by selecting the composition, dielectric matrix, and interparticle distances of narrow and shaped nanoparticles.[11,12] Therefore, among the plasmonic noble metals, Ag has attracted great attention due to its localized sharp and distinct SPR in the visible light region. In plasmonic materials, a transparent silicate glass embedded with nanoscale Ag metal is one of the best choices due to its third-order nonlinear susceptibility and ultrafast effect.[13,14] Therefore, the soda-lime glass matrices have been used as advanced host matrices for growing metal clusters on the nanoscale due to their mechanical strength, higher transparency, and easy fabrication. The arrays of metallic nanoclusters could be oriented under thermal or irradiation environments for producing a fine size distribution of nanosize particles inside the soda-lime glass matrix. Currently, various methods have been reported for the synthesis of Ag nanoparticles embedded in a glass matrix, such as ion implantation, melt-quench techniques, low-energy ion-beam mixing, physical vapor deposition, laser ablation, and ion exchange.[15,16] The synthesis methods have been reported with few demerits, but the ion-exchange method, which we have chosen, needs less concentration with shorter time. Thereby, we have preferred to anneal the sample from 500 to 650 °C, with a higher precision and better size control, which is advantageous over other methods used.

In the light of the above, Ag nanoclusters embedded on a soda-lime glass matrix have been fabricated using 0.5% of $AgNO_3$ with 95.5% of $NaNO_3$. The Ag^+ ion exchange has been made within a short duration at 390 °C as compared to the reported work.[15] The chosen ratio of $AgNO_3$ and $NaNO_3$ is

Received: May 25, 2017
Accepted: July 24, 2017
Published: September 14, 2017

DOI: 10.1021/acsomega.7b00672
ACS Omega 2017, 2, 5748−5758

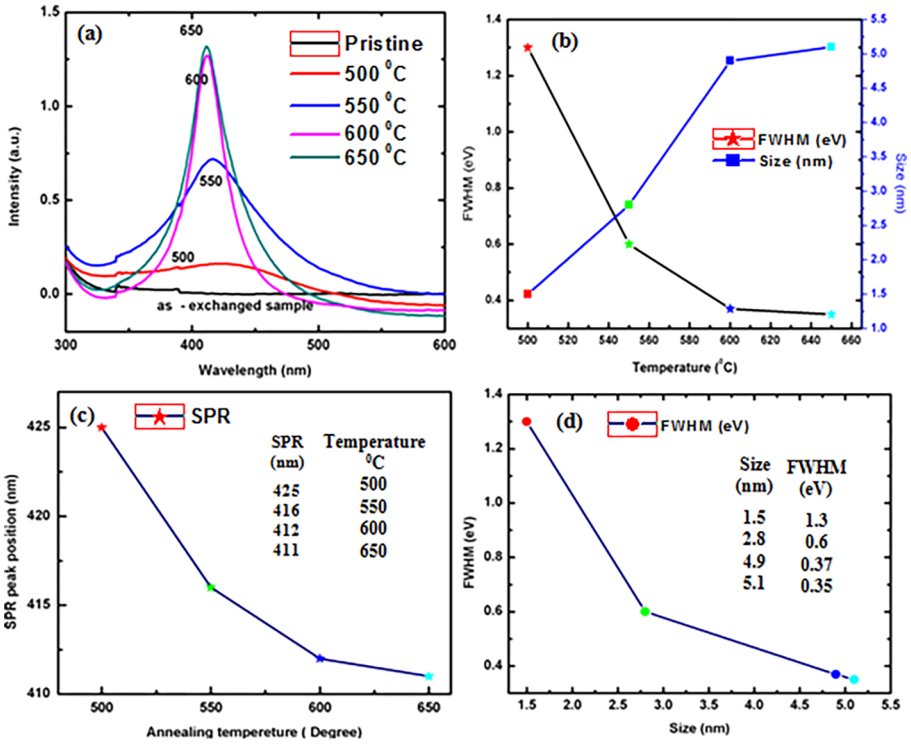

Figure 1. (a) SPR behavior of as-grown Ag nanoclusters at various temperatures. (b) Full width at half-maximum (fwhm) and particle size relation calculated by the Mie theory. (c) SPR response for annealed samples up to 650 °C. (d) Relation between size and fwhm for Ag nanoclusters. UV−vis spectroscopy analysis.

found adequate to reduce Ag^+ to Ag^0 in thermal conditions.[15,16] The Ag particles are structurally oriented as nanoclusters under uniform annealing (up to 650 °C) for 1 h inside the dielectric matrix. Therefore, the objective of our work has been to study the nanoclustering and tunable plasmonic behavior of the Ag-doped soda-lime glass. The structural, optical, and thermodynamic properties of as-grown Ag nanoclusters have been investigated and explained with mutual relevance. Such relevance is very useful to develop thermodynamic aspects for a thermally induced process by considering enthalpy, entropy, and Gibbs energy.[17,18] Moreover, thermodynamic measurements revealed the fundamental information about the physicochemistry of the growth mechanism, which has been explained under thermal conditions.[19−21] In contrast, the annealing temperature and time are both important factors for growing the material under controlled morphology with the surrounding environments. Thus, in a thermal process, the chemical and physical interactions of components regulate both the nucleation and the crystal growth with lattice orientations allowing the mass and heat-transfer phenomenon.[22,23]

2. RESULTS AND DISCUSSION

Figure 1 shows UV−vis spectra of pristine (ion-exchanged) and annealed samples at various temperatures for 1 h. The thermal interaction required to release electrons from the soda glass matrix for Ag^+ reduction to Ag^0, substantiated by higher thermal energy from 550 to 650 °C, seems to be accompanied with higher atomic or electronic energy involvement causing a blue shift. However, simultaneously the higher kinetic energy could have synergized the Ag dispersion vis-à-vis glass materials to place Ag^0 closely as a cluster of comparatively larger sized. Along with this, the needful fundamental science is incorporated in the article. It is seen that the pristine sample does not show any absorption band due to the ionic form of $Ag^+ \leftrightarrow Na^+$ exchanged inside the glass matrix or below 1 nm Ag particle synthesis at 390 °C for 5 min.[24] After annealing, the sharpened SPR intensity increases from 500−650 °C due to the thermal growth of neutral Ag particles inside the glass matrix (Figure 1a).

The substrate was considered as a host material that provided the required electrons for reduction of Ag ions into neutral Ag atoms. A temperature-driven mechanism was developed for the reduction process, and the source of electrons are discussed in the mechanism. In the process, initially Ag^+ was introduced to replace Na^+ inside the glass matrix. At higher temperatures, the electrons are captured from the silicate species of glass that used to reduce the Ag^+ to Ag^0. Moreover, the pure glass slide was used as the blank during the UV−vis spectra measurements, which nullified the substrate properties. Thus, an absorbance exists owing to the reduced Ag particles in UV−vis spectra. It is concluded that the higher population of reduced Ag atoms are formed with the ascending temperature, which reduces broadening of the SPR band at the visible region. As a result, a significant blue shift of 14 nm was observed from 425 to 411 nm, in the range of 500−650 °C (Table 1). It is already reported that the refractive index decreases at the glass surface

Table 1. SPR, fwhm, and Size Values of Ag Nanoclusters, with Respect to Temperatures

annealing temperature (°C)	annealing time (h)	SPR (nm)	fwhm (eV)	size (nm)
500	1	425	1.3	1.5
550	1	416	0.6	2.8
600	1	412	0.37	4.9
650	1	411	0.35	5.1

DOI: 10.1021/acsomega.7b00672
ACS Omega 2017, 2, 5748−5758

with increasing temperatures.[25] As compared to pristine Ag, a higher Ag population occurs at 500−650 °C on transferring the higher kinetic energy, where the medium itself becomes highly mobile rather than emitting rays, so the refractive index decreases. The structurally oriented reduced Ag atom arrays produce a lower refractive index from 500 to 650 °C. An effect of thermal treatment for controlling the size of Ag nanoclusters inside the glass matrix was investigated by the Mie theory calculation (Figure 1b−d). For the small clusters <10 nm, the decrease in fwhm with increasing cluster size is due to the mean free-path effect of electrons.[26] For a higher blue shift from 500 to 650 °C, the shorter λ_{max}, a free mean path is generated. However, the shorter mean free path indicates $Ag^+ \rightarrow Ag^0$ reduction at 500−650 °C due to oscillated electronic encounters caused by enhanced surface Ag dispersion. The plasmonic behavior of Ag nanoclusters, which are well dispersed in the transparent glass matrix and depend on size-dependent permittivity $\varepsilon(\omega, R)$ and absorption extinction (K) of Ag nanoparticles, where $R > \lambda$ and λ is the wavelength of light, is given by the following equation under quasistatic or dipole−dipole approximation.[25]

$$\varepsilon(\omega, r) = \varepsilon_1(\omega) + i\varepsilon_2(\omega, r) \quad (1)$$

The Mie theory resonance occurs when $\varepsilon_1(\omega) = -2\varepsilon_m$. When the Mie theory is fulfilled, the light field induces a resonant coherent oscillation of free electrons across the metal nanoparticle.

The optical coefficient (α) for metal (Ag) nanoparticles surrounded by the dielectric medium is expressed as[36,37]

$$\alpha = 9\frac{\omega}{c}\varepsilon_m^{3/2}V\frac{\varepsilon_2(\omega)}{[\varepsilon_1\omega + 2\varepsilon_m]^2} + \frac{1}{\varepsilon_2(\omega)^2} \quad (2)$$

where ε_m is the dielectric constant of the medium, V is the volume fraction of metal particles, which is small compared to the imposed light wavelength (λ), and ε_1 and ε_2 are frequency-dependent real and imaginary components that could be expressed by the optical constant of their bulk metal.[38] The dielectric function $\varepsilon(\omega, R)$ for metal nanoparticles can be given as

$$\varepsilon(\omega, R) = \varepsilon_{bulk}(\omega) + \omega_p^2\left(\frac{1}{\omega^2 + \Gamma^2} - \frac{1}{\omega^2 + \Gamma(R)^2}\right) - i\frac{\omega_p^2}{\omega^2}\left(\frac{\Gamma(R)}{\omega^2 + \Gamma(R)^2} - \frac{\Gamma}{\omega^2 + \Gamma^2}\right) \quad (3)$$

Where Γ and $\Gamma(R)$ are relaxation time for the bulk metal and size-limited time, respectively, and ω_p is the Drude plasma frequency in bulk metal. The Drude plasma frequency depends on the electron density (n) of electron effective mass (m_e), N is free electrons per unit volume (Ag, $\omega_p = 5.17 \times 10^{15}\ s^{-1}$), $\nu_f = 1.39 \times 10^6$ m/s is the Fermi velocity for bulk silver, and C is the volume concentration of the embedded particles.

The resonance condition is satisfied only for the Ag nanoparticles in the visible wavelength range. This is basically the origin of their intense color, as shown in Figure 1. The average size of Ag nanoclusters is calculated with the equation given below.

$$d = 2V_f/\Delta E_{1/2} \quad (4)$$

where d is the average size of the particle, V_f is the Fermi velocity of electrons of bulk Ag (1.39×10^6 m/s), and $\Delta E_{1/2}$ is the fwhm of SPR band. The data are in close agreement for a size of Ag that is smaller than the free mean path of electrons, which is 27 nm at room temperature (RT) (25 °C) for the bulk Ag.[26] The particle sizes calculated by UV−vis absorption spectra based on the Gaussian profile are 1.4, 2.8, 5.2, and 6.1 nm for 500, 550, 600, and 650 °C, respectively (Figure 1b).

Figure 2 shows PL spectra of the as-exchanged and thermally annealed Ag^+−Na^+ ion-exchanged glass samples at various temperatures for 1 h. The PL spectra were recorded at 325 nm excitation wavelength at RT for all samples. The PL intensity decreases systematically on turning toward higher annealed temperatures at 500, 550, 600, and 650 °C respectively. The pristine sample shows higher intensity due to higher Ag^+ ionic population, which exists on the glass substrate initially, but the intensity decreases systematically from 500 to 650 °C as the Ag^+ ionic species converts into Ag^0 atoms under the thermal growth process.[27] Moreover, the opacity of Ag nanoclusters dispersed in soda-lime glasses increased (very faint to dark yellow) with increasing annealing temperatures (Figure 2a). It has earlier been studied that the no emission spectra were recorded for the neutral Ag^0 atom in any excitation wavelength, whereas the Ag^+ ions show luminescence behavior in both the bulk crystal structure and the glass matrix.[27] On increasing annealing temperatures, the decreased PL intensity has confirmed a fast growth of Ag^0 atoms on the glass matrix, which might be the reason for reducing the PL intensity. The luminescence properties of pristine and annealed samples under 325 nm have been identified using Commission Intemational de l'Eclairage (CIE) chromaticity study (Figure 2b). The emission spectra of Ag-embedded samples were converted to CIE chromaticity using PL data. The pristine samples show a

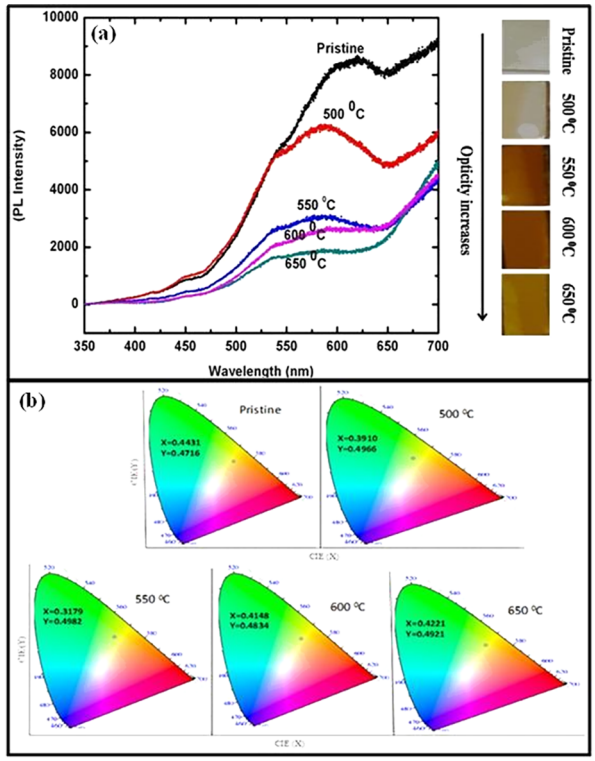

Figure 2. (a) PL spectra of pristine and annealed samples with opacity order, (b) the CIE diagram for pristine and annealed samples from 500 to 650 °C for 1 h. Photoluminescence (PL) spectra.

DOI: 10.1021/acsomega.7b00672
ACS Omega 2017, 2, 5748−5758

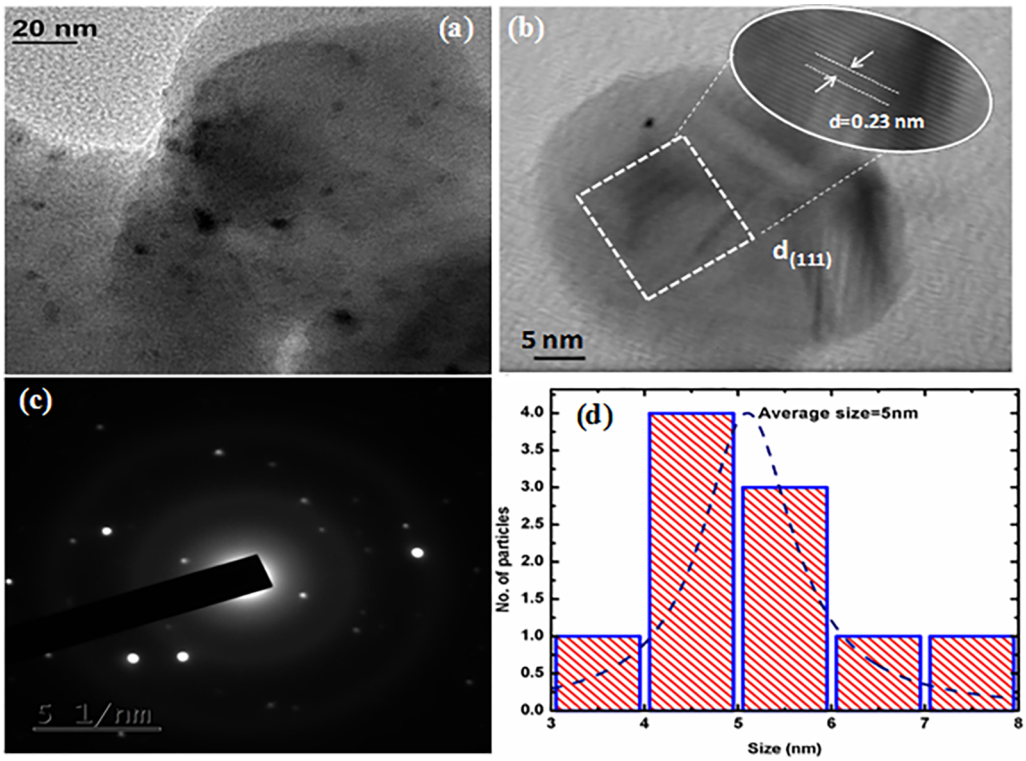

Figure 3. (a) TEM image of Ag nanoclusters. (b) HRTEM image of Ag nanoparticles. (c) The SAED pattern of Ag nanoparticles at 650 °C (d) Histogram for average particle size distribution. Morphology analysis by HRTEM.

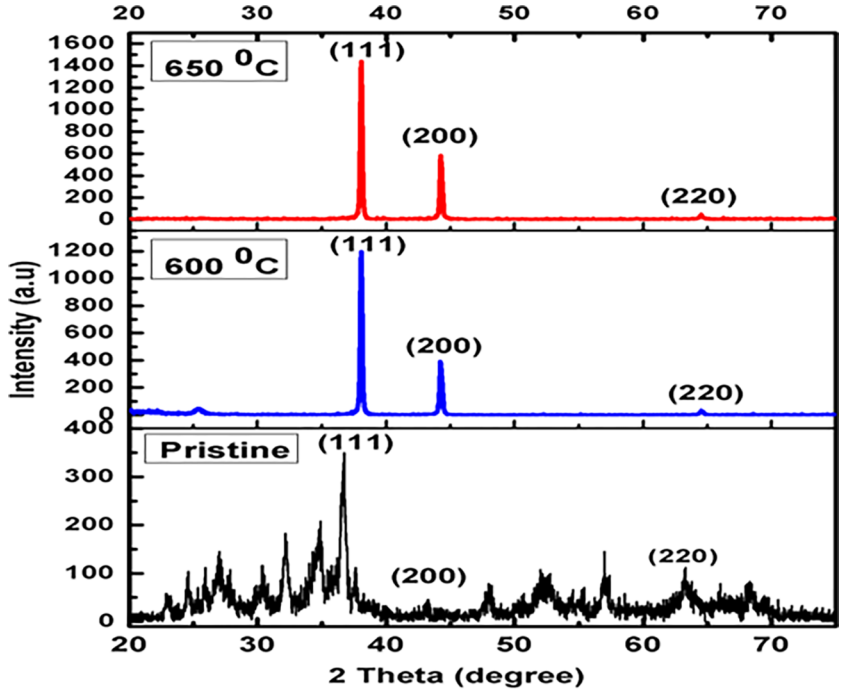

Figure 4. XRD diffraction pattern of Ag-ion exchanged (pristine) and annealed samples at 600 and 650 °C. The XRD profile of pristine and annealed samples.

yellow region compared with annealed samples as the latter shows a blue shift, which is also exhibited in UV−vis spectra. The CIE diagram shows an optical change in the visible range due to size variations at different temperatures. The shifting of color in the CIE graph indicates a blue shift observed from 500 to 650 °C (Figure 2b), which is in close agreement with UV−vis blue shifts. This study helps to observe the opacity change in Ag-embedded glass materials due to change in absorbance and scattering of diffused and accumulated Ag particles. This is the reason that we have used the CIE study with PL data in our work. These optical results indicate that the as-embedded Ag nanostructures show multicolor emissions over the visible zone

DOI: 10.1021/acsomega.7b00672
ACS Omega 2017, 2, 5748−5758

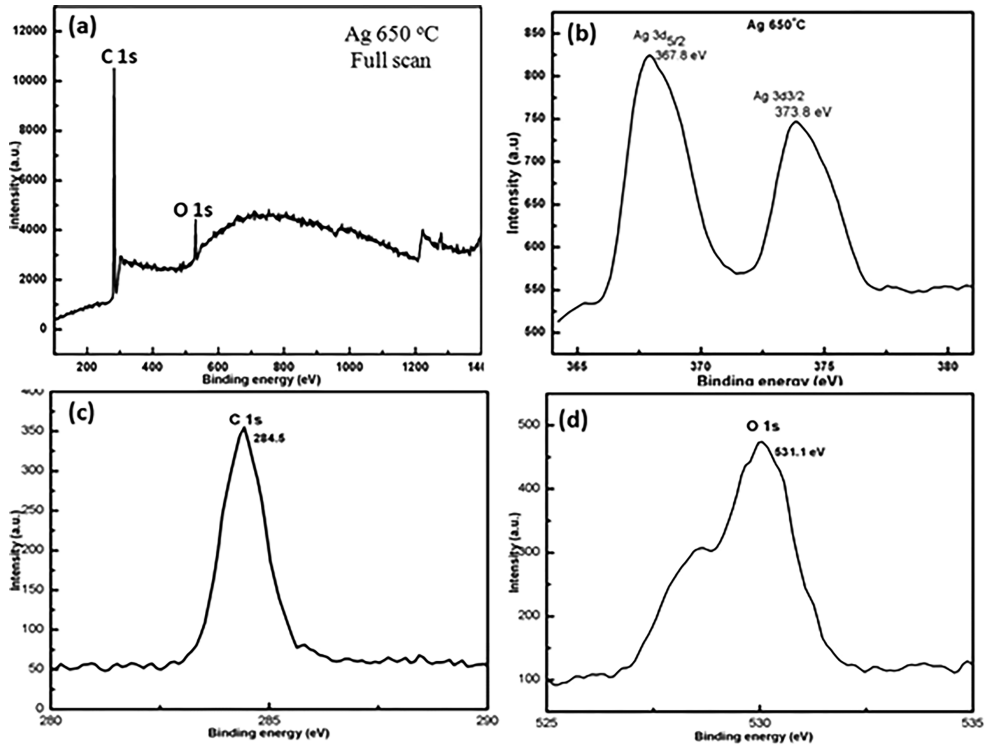

Figure 5. XPS spectra of the Ag-embedded annealed sample at 650 °C. (a) Full survey scan spectra. (b) Ag 3d core-level spectra. (c) C 1s core-level spectra. (d) O 1s core-level spectra. XPS spectroscopy analysis.

when they are induced by the single-wavelength light. These optical properties could be used in several applications like optoelectronic, bioimaging, and light emitting diodes.

For the morphology, transmission election microscopy has been performed for an Ag-embedded glass-annealed sample at 650 °C, which was mounted on a carbon-coated copper grid with 200 mesh. Figure 3 shows TEM images of spherical Ag nanoclusters embedded in the glass matrix after thermal growth (Figure 3a). The 5 nm average size is calculated from the TEM images at 650 °C (Figure 3d) and reported already, which is in close agreement with the UV−vis size calculated by the Mie theory (Figure 1b,d). Several researchers have also reported TEM images for lower temperatures (2.9, 4.4 nm at 550 and 600 °C), which were correlated with the 650 °C annealed sample in our study.[47] Both the high-resolution transmission electron microscope (HRTEM) image and selected area electron diffraction (SAED) pattern (Figure 3b,c) were analyzed, which shows spherical Ag nanoparticles. The particles show a crystalline nature as they are grown at higher temperatures with (111) crystallographic planes that have 0.24 nm *d*-spacing for Ag^0 nanoparticles.[28,29] The UV−vis results show the intense peaks that might have come out due to spheres of Ag^0 particles that could be of equal distribution. Thereby, we have applied the Mie theory for size determination of metallic Ag particles and not the metal oxide (Ag_2O). The metallic crystalline nature was confirmed with SAED patterns, and the shape is analyzed by TEM images that show spherical Ag particles. The shape, size, and distribution are investigated under the nanorange for Ag^0 particles because the plasmonic properties are tuned by the size and distribution pattern of the particles in the glass substrate.

The X-ray diffraction (XRD) patterns were analyzed for the pristine and annealed samples at 600 and 650 °C for 1 h. The XRD profile of a pristine sample shows few extra peaks due to the glass compositions and glassy behavior of the ion-exchanged sample at 390 °C (Figure 4). The annealed samples show a very sharp and high intense peak due to the rapid thermal growth of Ag nanoclusters with (111), (200), (220), and (311) crystallographic planes and the FCC crystalline structure with respect to 38.2, 44.3, 64.6, and 77.2° values (JCPDS file no. 00-004-0783) (Figure 4).[30] Thus, the thermal effects play a significant role for both the nucleation and growth of Ag nanoclusters inside the glass matrix. At 390 °C, that is, before annealing a sample, the extra peaks have appeared in XRD spectra of the pristine sample, which may be due to the presence of Ag_2O at 32.7° on the 2θ scale (ICCD Card No: 00-41-1104) along with glassy contents, such as Fe_2O_3, at around 57, 54° (511, 422), Al_2O_3 46° (400) (JCPDS 10-0425) and MgO at 42° (200) (JCPDS- 01-1235).[31−33] Remarkably, on completely annealing from 600 and 650 °C, the glass matrix did not show these peaks in XRD spectra, which could be due to a higher distribution of Ag neutral atoms diffused on the glass surface at 600 and 650 °C. However, the annealed sample at 600 °C showed a comparably less intense peak than that at 650 °C, which indicates the higher diffusion and accumulation of Ag nanoclusters on the glass surface at the applied temperature (Figure 4). Thus, the particle sizes are controlled under thermal effects and the crystalline sizes of Ag nanoclusters were calculated using the Scherrer equation with respect to different temperatures. The obtained sizes are 8.9 and 8.3 nm for the 650 and 600 °C annealed samples using the Debye−Scherrer formula (Figure S4). Thus, on increasing the annealed temperature, the sizes are increased because of the larger clustering of reduced Ag particles. The obtained sizes are 8.9 and 8.3 nm for the 650 and 600 °C annealed samples in XRD results, respectively, using the Debye−Scherrer formula (Figure S4). Thus, on increasing the annealed temperature, the sizes are increased because of the larger clustering of the reduced Ag

DOI: 10.1021/acsomega.7b00672
ACS Omega 2017, 2, 5748−5758

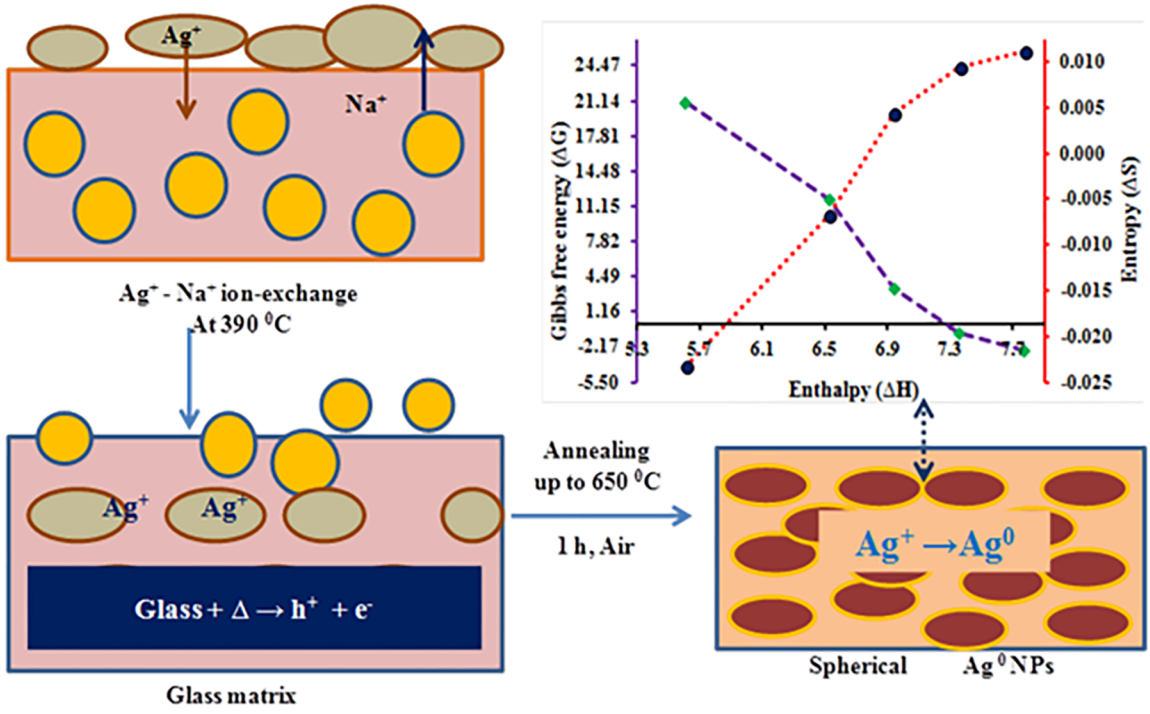

Figure 6. Schematic representation for thermal growth of Ag nanoclusters within soda-lime glass. The thermal growth mechanism for Ag nanoclusters within the glass matrix.

particles. These results are close to the UV−vis sizes (5.2 and 6.2 nm) for 600 and 650 °C, whereas the TEM images show a 5 nm average size, which is in agreement with XRD and UV−vis sizes. At higher temperatures, the XRD peaks (38.2, 44.3, 64.6, and 77.2°) support the presence of Ag particles and not Ag_2O, which infer a pure Ag nanocluster formation. These results are correlated with the spectra of X-ray photoelectron spectroscopy (XPS), where the eV for the splitting of $^3d_{5/2}$ and $^3d_{3/2}$ of the Ag^0 atom are present at 650 °C. These splitting energies are closely matched with the XPS of the literature values reported for the Ag atom.[34,35] Consequentially, the pristine sample shows comparably broad and less intense peaks, with some additional peaks due to the presence of glassy compositions with less Ag particles. However, the annealed samples show highly intense and sharp peaks due to larger Ag^0 population on the glass surface. The oxidation state of Ag particles is confirmed by XRD and XPS, where the neutral Ag particles were found at higher temperature. In the pristine sample, Ag_2O could be present because an ion-exchange process was conducted in open air at 390 °C. However, at 650 °C, due to higher kinetic energy, the oxygen could have escaped out of the chemical process of ion exchange. Thus, the Ag_2O peak is not seen in XRD spectra.

The XPS spectra were recorded for the investigation of in situ diffusion of Ag atoms toward the glassy surface under thermal treatment. In XPS measurement, the core-level photoelectron binding energy was initially calibrated by the surface carbon C 1s at 284.6 eV. Figure 5 shows Ag 3d XPS spectra of the Ag annealed sample at 650 °C for 1 h. The thermal growth of Ag nanoclusters identify with XPS spectra of core-level Ag 3d signals, which reveal the thermal diffusion of Ag atoms on the surface at higher temperatures. Binding energy of the annealed sample is located at 368.0 and 374.1 eV, corresponding to spin−orbit splitting of Ag $^3d_{5/2}$ and Ag $^3d_{3/2}$, respectively (Figure 5b). The located peak of Ag 3d at the core-level spectrum confirmed the presence of neutral silver in metallic form in the glass host and showed 6.0 eV differences[34,35] between the two major Ag peaks. The results confirmed that Ag^+ ionic atoms are reduced as Ag neutral atoms and diffuse toward the glass surface as nanoclusters under thermal treatment. The expected elements like C and O are present due to the atmospheric environment, where the O atom occurred may be due to the SiO_2 content of the glass matrix. For the annealed sample at 650 °C, the Ag 3d peaks were observed at 368.0 and 374.1 eV corresponding to the spin−orbit splitting of Ag $^3d_{5/2}$ and Ag $^3d_{3/2}$ (Figure 5b), respectively, whereas the pristine sample did not show the Ag 3d peak because there is no reduced Ag atom on the glass surface at 390 °C. The AgO XPS peaks are reported at 368.2 eV, which is not found in the 650 °C annealed sample because of a complete reduction of Ag^+ to Ag^0. So it is considered that the reduced Ag atoms are diffused toward the surface at higher temperatures rather than the Ag oxide species. Ag^0 is not observed in the full scan because the C and O peaks are prominent as compared to Ag atom, but by selecting the binding energy of core Ag 3d determined with XPS, the peak is observed at 650 °C due to spin-splitting in the orbit of Ag $^3d_{5/2}$ and Ag $^3d_{3/2}$. So in XPS full survey scan spectra, the carbon C 1s peak appeared due to a natural contaminant reaching the vacuum chamber of the XPS instrument (Figure 5). The O 1s peak appeared at 531.1 eV, which may be assigned to SiO_2 of the glass matrix (Figure 5d).

3. THERMAL GROWTH MECHANISM FOR AG NANOCLUSTERS INSIDE THE GLASS MATRIX

During the ion-exchange process, the Ag^+ ions are incorporated into the host matrix by substituting Na^+ at 390 °C to form Ag^0 in a small amount. Under the thermal conditions (up to 650 °C), the Ag ions reduced to neutral Ag atoms by capturing the required electrons from the glass matrix,[39] especially from the

DOI: 10.1021/acsomega.7b00672
ACS Omega 2017, 2, 5748−5758

silicate species (Figure 6). The population of Ag nanoparticles depends upon a fractional volume of Ag^+ ions, which requires sufficient electrons from the host material. The proposed mechanism infers that the required electrons are captured from the glass-containing atoms, especially the intrinsic oxygen.[40] The thermal reduction of Ag ions into Ag neutral is explained in the growth mechanism, where the available electrons have reduced the Ag metal represented as:

Temperature driven mechanism for Ag nanocluster

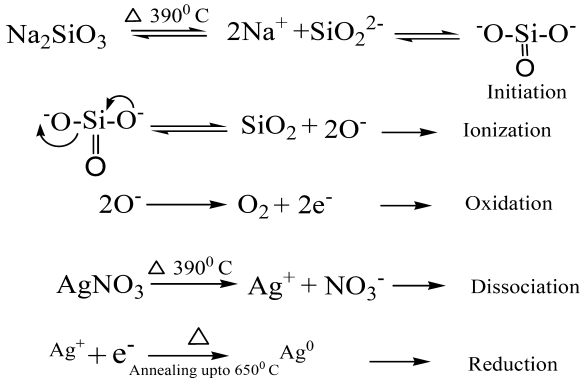

The Ag^+ ions are reduced into Ag nanoclusters on capturing the electrons as per requirements, leading to higher population of Ag nanoclusters under the annealing conditions. The Ag atoms with higher kinetic energy diffuse on the glass surface at higher temperatures because of the thermal relaxation of surface tensile stress. Ag^0 accumulation with the relaxation produces the Ag nanoclusters on the glassy surface after cooling the annealed samples at RT for 5−6 h. Such spatial Ag nanocluster arrangements vis-à-vis thermal reduction induce thermodynamic changes. Thus, we have reported enthalpy (ΔH), entropy (ΔS), and Gibbs energy (ΔG), as the metallic nanomaterials were prepared under thermal process (Table 2). We have also observed the initiation, ionization, reduction, dissociation, and oxidation processes systematically under a thermally driven mechanism for Ag nanoclusters' growth. Thus, our work explored new information for developing advanced metallic embedded nanomaterials by dispersing noble metals in the dielectric medium on thermal treatments.

Table 2. ΔH, ΔS, and ΔG Values for Pristine and Annealed Samples

absorbance	T (K)	E_a (J/mol)	ΔH (kJ/mol)	ΔG (kJ/mol)	ΔS (J/mol)
1.39	923.15	97.70	7.77	−2.53	11.16
1.12	873.15		7.36	−0.82	9.37
0.61	823.15		6.94	3.38	4.32
0.16	773.15		6.53	11.78	−6.80
0.02	663.15		5.62	21.05	−23.28

4. THERMODYNAMICS FOR THERMALLY STRUCTURED AG NANOCLUSTERS INSIDE THE GLASS MATRIX

As the Ag nanoclusters are grown and reoriented under the temperature-driven mechanism, the thermodynamic properties are studied. Such studies are relevant for basic understanding of Ag^+ to Ag^0 reduction, with thermally realigned Ag nanoclusters within the matrix. Ag^+ ions require sufficient energy to overcome the static barrier potential at a low temperature, which could be considered as the bonding energy of Ag−O in the matrix. This required energy is noted as activation energy (E_a), which plays a key role for the thermal growth of Ag clusters. Thus, we have studied the activation energy with the enthalpy (ΔH), entropy (ΔS), and Gibbs energy (ΔG) values for pristine and annealed processes (Table 2). Moreover, Ag^+ to Ag^0 were thermally dispersed in the glass matrix and precipitated as Ag nanoclusters at various temperatures. Thus, both the diffusion and accumulation of the Ag atoms increase at higher temperatures, which could have caused a change in optical properties by light scattering and absorbance of diffused Ag atoms[41] and are adequately focused on in this study.

In the UV−vis absorbance measurement, pure soda-lime glass slide is used as the blank sample which nullified the glass (substrate) properties for the optical density. Thus, the optical absorbance exists through the Ag particles that are embedded or diffused on the glass surface. So it is clearly justified that the optical density is considered due to the reduced Ag atoms. Consequently, we have used optical absorbance as the authentic data for calculation of activation energy and other thermodynamic parameters for Ag nanocluster growth. So UV−vis absorbances are used to detect the changes in the form of optical density, as experimentally observable signals. The optical density or absorbance is used as authentic data to calculate the activation energy along with other thermodynamic properties (Figure 7). The activation energy is calculated using

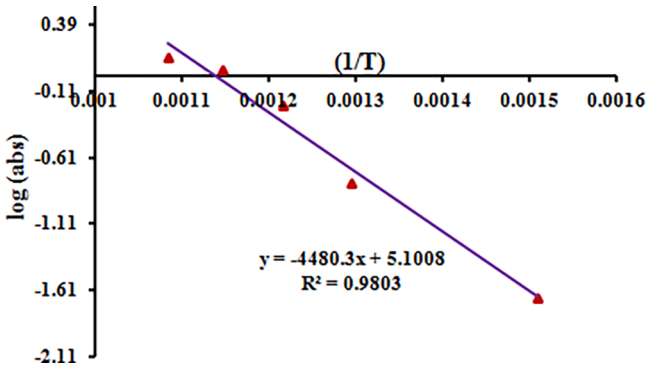

Figure 7. Activation energy of the Ag-embedded glass sample at variable temperatures. Activation energy calculation.

the Arrhenius equation (Figure S3) on increasing the temperature and fitted as

$$\log(\text{abs}) = \log A - \frac{E_a}{2.303R} \text{ or } \log(\text{abs}) = \log A - \frac{E_a}{2.303R}\frac{1}{T} \quad (5)$$

where abs is the absorbance, T is the temperature (kelvin), R is the gas constant (8.314 J/(mol K)), A is the frequency factor, and E_a is the activation energy (J/mol). Log(abs) versus $1/T$ plot of the Arrhenius equation is a straight line with $(-E_a/R)$ slope, depicting Ag^0 diffusion on the glass matrix as the first order process (Figure 7). The reduction from Ag^+ to Ag^0 and diffusion of Ag^0 toward the surface depends on the activation energy, which is the essentially required energy for breaking Ag−O bonds during the annealing process. Because Ag^0 is featured by optical absorbance, the absorption is noted as an authentic experimental variable for calculating E_a. Further, this

DOI: 10.1021/acsomega.7b00672
ACS Omega 2017, 2, 5748−5758

E_a is used to calculate the ΔH for the pristine and annealed processes given under

$$\Delta H = E_a - 2.303RT \quad (6)$$

The temperature effect on pristine and annealed samples have been investigated; the absorbance versus temperature relation furnishes information about the kinetic rate for Ag^0 nanoclustering and derives thermodynamic parameters of the growth mechanism. So the Gibbs energy (ΔG) and entropy (ΔS) for Ag clustering are calculated using equations (Figure S3) given as

$$\text{entropy } (\Delta S) = \frac{(E_a - 2.303RT + 2.303RT \log(\text{abs}))}{T} \quad (7)$$

Equation 7 is modified as under

$$\Delta S = \left(\frac{E_a}{T}\right) - 2.303R[1 - \log(\text{abs})]$$

Because the UV−vis absorbance inferred the transformation from $Ag^+ \rightarrow Ag^0$, it is used as a variable in the equation for calculating the Gibbs energy (ΔG)

$$\Delta G = -2.303RT \log(\text{abs}) \quad (8)$$

where, the symbols are usual for Ag nanoclustering under the applied thermal treatment, respectively, at both adequate activation energy and Gibbs energy. The chosen thermodynamic parameters have supported the thermal nanoclustering of Ag in the glass matrix.

The above mechanism has inferred an enthalpy change which could illustrate an internal arrangement of Ag nanoclusters. The positive ΔH from 5.62 to 7.77 kJ/mol depicts growth and nucleation processes for pristine and annealed samples (Table 2). From 390 to 650 °C, for the annealing process, ΔH becomes more endothermic on decreasing ΔG from 923.15 and 873.15 K, which indicates a spontaneous process (Table 2). Further, increasing positive ΔH values and similarly decreasing ΔG values directly reflect a coercive thermodynamic energy exchange from 390 to 650 °C (Figure 8). Such a valuable thermodynamic relationship creates a vacancy and elucidates the need of kinetic energy for transforming Ag^+ to Ag^0 owing Ag−O bond breaking and arranging the Ag atoms in an FCC phase with higher crystallinity. This kinetic energy enhances the nucleation of a larger population of Ag atoms[42,43] into the FCC crystal lattice. Thereby, on forming the (111), (200), (220), and (311) crystallite planes, polycrystallinity of the Ag nanocluster samples are depicted from XRD analysis (Figure 4). Table 2 reports the entropy of the process from 390 to 650 °C, where the high annealing temperature is associated with positive entropy as compared to the negative entropy at lower temperature. These results support the findings obtained from the XRD analysis, where the FCC (111), (200), (220), and (311) planes of Ag are absent in the pristine sample (at T = 663.15 K), whereas the crystallographic planes are present in annealed samples at higher temperatures (Figure 4). The presence of lattice planes of Ag nanoclusters, which is diffused in the glass, reflects a less ordered arrangement with positive entropy. The higher temperature facilitates the presence of variable crystalline plane orientations with a randomized direction of atomic arrangements.

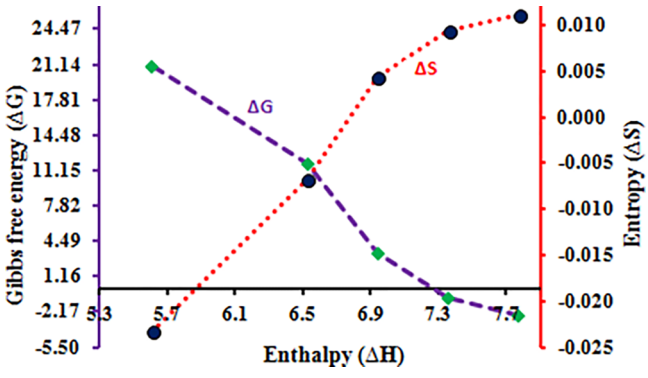

Figure 8. Kinetic model for enthalpy, entropy, and Gibbs free energy for pristine and annealed samples. ΔH, ΔS, and ΔG relations for thermal growth of Ag nanoclusters.

The positive ΔS values for annealing depict favorable entropic changes with increased Ag^0 population. Both the ΔH and ΔS values show an optimized energy, with a mutual relationship of the enthalpy−entropy compensation phenomenon. Such trends depict causing either the higher ΔH absorption or release, and in both cases, the ΔS increases and decreases accordingly. Thus, their mutual relationship depicts a partitioning of Ag^0 in the glass matrix in spatial orientations. A significant mutual relation among ΔG, ΔH, and ΔS reveals the thermal growth and clustering behavior of Ag atoms in the process (Figure 8). On increasing ΔH, ΔS is increased due to the required thermal energy transformation during the bond breaking and making process for the Ag−O and Ag−Ag inside the glass matrix. Thus, the enthalpy is increased for reduction and clustering of the reduced Ag atoms through the redox and Ag clusters reorientation phenomenon. However, ΔS is increased due to a stronger nanoclustering of reduced Ag atoms at higher temperature, which forms Ag−Ag bonds. These two thermodynamic parameters collectively infer the thermal growth and clustering behavior, which utilizes almost all energy in the process of balancing the minimum energy of the system. It is well documented that the spontaneity of any chemical reaction could be represented by ΔG values.[44] So in our work, we have explained the dependence of ΔG in favor of Ag clustering within the dielectric matrix. Also, at a very high temperature as well as higher kinetic energy, the Ag atoms tend to self-accumulate as nanoclusters. The thermodynamic synergy among ΔG, ΔH, and ΔS data are not independent to each other but are interdependent. In our studies, the Ag-embedded glass materials were subjected from 500 to 650 °C, where Ag^+ converts to Ag^0. The ΔH, ΔS, and ΔG properties along with E_a are calculated using optical absorbance at different temperatures. The trend and magnitude of the ΔH, ΔS, and ΔG model is developed for nucleation and growth of Ag^0 under the thermal process.

5. CONCLUSIONS

The Ag nanoclusters were grown and nucleated in a glass matrix by an ion-exchange process, followed by thermal annealing from 500 to 650 °C. The Ag ions are reduced into neutral silver atoms (Ag^0), and subsequently Ag^0 atoms are diffused toward the surface under thermal treatments. The SPR behavior with different sizes are calculated and explained by the Mie theory using UV−vis measurements at various temperatures. Lower photoluminescence intensity on increasing temperatures is attributed to the reduction of Ag^+ to Ag^0 atoms on the glass matrix. The XRD results have confirmed the FCC crystalline structure of Ag metal after annealing the

DOI: 10.1021/acsomega.7b00672
ACS Omega 2017, 2, 5748−5758

samples at 600 and 650 °C for 1 h. HRTEM images have revealed the presence of spherical Ag nanoparticles (d_{111} = 0.23 nm), with a maximum particle size of 5 nm at 650 °C, which is consistent with the Mie theory sizes. The oxidation state of Ag^0 has been confirmed by XPS spectra located at Ag $^3d_{5/2}$ and Ag $^3d_{3/2}$ spin−orbit splitting for Ag nanoclusters at 650 °C. Thermodynamic studies are made for a thermal process with 97.70 kJ/mol of activation energy. The entropy, enthalpy, and Gibbs energy are arrived at from optical absorbance considered as experimental authentic results, which help to understand the thermal mechanism for reduction and nucleation of Ag nanoclusters.

6. EXPERIMENTAL SECTION

6.1. Materials. Chemical reagents, such as $AgNO_3$ (99.0%) and $NaNO_3$ (99.0%), were procured from Sigma-Aldrich. Commercial (Blue Star Company, India) soda-lime glass with weight-percent-wise composition of 72.0% SiO_2, 14.0% Na_2O, 0.6% K_2O, 7.1% CaO, 4.0% MgO, 1.9% Al_2O_3, 0.1% Fe_2O_3, and 0.3% SO_3), with 1 mm thickness, was used as the host matrix. AR grade solvents were used for cleaning of the samples in the whole experiment.

6.2. Synthesis of Ag Nanoclusters. The ion-exchange ($Ag^+ \leftrightarrow Na^+$) route was performed for Ag nanoclusters synthesis in a soda-lime glass. The Ag-embedded glass material was prepared by an ion-exchange method, followed by a thermal annealing at air atmosphere. Soda-lime glass was chosen as the dielectric host matrix for Ag nanoclusters growth. First, the glass slides were poured in formic acid for 15 min to remove the impurities from the slide surface. Later, the poured glass slides were cleaned with distilled water, acetone, and trichloroethylene by ultrasonication (20 kHz) for 15 min. Now, the homogeneous mixture of 0.5% $AgNO_3$ and 95.5% $NaNO_3$ was prepared by molten piston grinding. The glass slide pieces were kept in an alumina boat (Al_2O_3 > 99%) and filled with a grinded homogeneous mixture of $AgNO_3$ and $NaNO_3$ precursors. The alumina boat was transferred into a tubular furnace for Ag and Na ion-exchange inside the glass slide at 390 °C for 5 min (Figure SI1). During this short duration, the Ag^+ ions diffuse inside the glass by replacing the Na^+ ions; the details are given in Figure 6. After ionic in situ diffusion the as-ion-exchanged samples were cooled at room temperature and then cleaned with distilled water and acetone for removing the rest of the adhering part of $AgNO_3$ on the glass surface. The as-ion-exchanged (pristine) samples were faint yellow or colorless, and such optical behavior is observed due to in situ diffusion of ionic species (Ag^+/Na^+) with different sizes, mechanical stress, and change in electrical polarization of diffused ions in glass. Further, the cleaned pristine samples were annealed from 500 to 650 °C for 1 h so that the glass melting point is maintained to prevent glass. At lower temperatures, few Ag^+ ions are formed by Ag−O bond breaking in the matrix but for diffusion on the surface, the higher energy is required to move the ions toward a more relaxed surface. Thus, on increasing temperature, the larger Ag segregation and diffusion was done on the glassy surface and it could be understood by the size difference in Ag^+ and Na^+ (ionic radius ratio, r_{Ag^+}/r_{Na^+} is 1.29).[45,46] Our work is compared and discussed with respect to annealing studies of Ag particles collected from $AgNO_3$ as precursor. These studies were conducted at 600 °C as reported elsewhere, and we have used a less concentration as compared to that in the reported work,[47] where the samples were annealed up to 650 °C. The effect of temperature on size and plasmonic properties were investigated up to 650 °C, which is advanced than that in the reported work. Noticeably, we have investigated the thermodynamic properties accompanied with a thermal growth of Ag nanoclusters at different temperatures, which is not reported by other researchers who had followed the ion-exchange route. Contrary to others, we have determined entropy, enthalpy, and Gibbs properties, which are the most intricate probes and critically undergo a change in their magnitudes vis-à-vis structural states of the Ag nanoclusters. Thereby, our thermodynamic model could be proven to be a pioneering one.

It is of key importance to find thermodynamic properties because of the thermal process followed for Ag diffusion and their clustering. Thus, the activation energy is estimated with Gibbs energy, which helps to produce the Ag atoms due to energy difference of pure Ag and Ag−O inside the glassy matrix. The Gibbs free energy of Ag−O is lower than that of the pure Ag, and this difference could have caused a dissociation of Ag−O bonds to form Ag−Ag bonds that favor the minimum energy state.[48] Thus, it is clear that the thermodynamic behavior of Ag diffusion by energy loss and thermal relaxation of surface stress are caused by the radius difference between Ag^+ and Na^+ (r_{Ag^+}/r_{Na^+} is 1.29). The thermal growth mechanism for Ag nanoclusters inside the glass matrix is schematically investigated, and its chemical reaction is explained in Figure 6. The annealed samples were taken for their structural and optical behavior in thermodynamic studies. The pristine and thermal annealed samples were characterized by UV−vis, PL, XRD, XPS, and HRTEM techniques for the optical, structural, and elemental confirmation.

The growth process of Ag nanoclusters embedded in glass were optimized by thermal annealing using a tubular furnace from 500 to 650 °C. The plasmonic properties were studied by dual beam UV−vis spectroscopy (spectro 2060 plus) from 300 to 800 nm wavelength, and the pure soda-lime glass was taken as a reference sample for UV−vis measurements. The PL measurements were carried out by the Fluoromax Photoluminescence spectrometer at 325 nm excitation wavelength for all samples. The shape and size of Ag nanoclusters were studied with HRTEM (JEOL TEM 2100) operated at 200 kV accelerating voltage. The Ag-embedded glass sample was crushed via pestle and mortar to form fine powder, and then a few milligrams of the powder was dispersed in ethanol under ultrasonication for 30 min. The few drops of the upper suspension were placed on carbon copper-coated grid with 200 mesh for analysis. The crystal structures of pristine Ag and Ag nanoclusters diffused on a glass substrate were confirmed by XRD analysis (Bruker D8 diffractometer using Cu Kα irradiation (λ = 1.54060 Å). XPS measurements were performed using Omicron Nanotechnology ESCA plus (electron spectroscopy for chemical analysis) with UHV twin anode Al Kα radiation of 1486.6 eV, generated by a 15 kV electron effect on the Al anode. The pass energy (20 eV) was applied for 0.5 eV resolutions during photoelectron scanning.

■ ASSOCIATED CONTENT

Supporting Information

The Supporting Information is available free of charge on the ACS Publications website at DOI: 10.1021/acsomega.7b00672.

Experimental details- materials and method, ion-exchange process, XPS spectra of the ion-exchanged

DOI: 10.1021/acsomega.7b00672
ACS Omega 2017, 2, 5748−5758

(pristine) sample, thermodynamic equations and XRD analysis (PDF)

AUTHOR INFORMATION

Corresponding Author

*E-mail: mansingh50@hotmail.com.

ORCID

Man Singh: 0000-0002-0706-3763

Notes

The authors declare no competing financial interest.

ACKNOWLEDGMENTS

Authors are grateful to the Central University of Gujarat for infrastructural support. RGNF is acknowledged for the SRF awarded (f1-17/2012-13ST-MAD-23445) to G.K.I. and (f1-17/2013-14SC-UTT-35366) Y.R. Authors are thankful to CeNSE IISc Bangalore for providing the instrumentation facility.

REFERENCES

(1) Knight, M. W.; Sobhani, H.; Nordlander, P.; Halas, N. J. Photodetection with active optical antennas. *Science* **2011**, *332*, 702−704.

(2) Lal, S.; Link, S.; Halas, N. J. Nano-optics from sensing to waveguiding. *Nat. Photonics* **2007**, *1*, 641−648.

(3) Jiang, Z. J.; Liu, C. Y.; Sun, L. W. Catalytic Properties of Ag Nanoparticles Supported on Silica Spheres. *J. Phys. Chem. B* **2005**, *109*, 1730−1735.

(4) Inwati, G. K.; Rao, Y.; Singh, M. In Situ Free Radical Growth Mechanism of Platinum Nanoparticles by Microwave Irradiation and Electrocatalytic Properties. *Nanoscale Res. Lett.* **2016**, *11*, 458.

(5) Giljohann, D. A.; Seferos, D. S.; Daniel, W. L.; Massich, M. D.; Patel, P. C.; Mirkin, C. A. Gold nanoparticles for biology and medicine. *Angew. Chem., Int. Ed.* **2010**, *49*, 3280−3294.

(6) Dong, J.; Zheng, H. R.; Li, X. Q.; Yan, X. Q.; Sun, Y.; Zhang, Z. L. Surface-enhanced Fluorescence from Ag Fractallike Nanostructures Decorated with Ag Nanoparticles. *Appl. Opt.* **2011**, *50*, G123−G126.

(7) McFarland, A. D.; Young, M. A.; Dieringer, J. A.; Van Duyne, R. P. Wavelength-scanned Surface-enhanced Raman Excitation Spectroscopy. *J. Phys. Chem. B* **2005**, *109*, 11279−11285.

(8) Allen, M. A.; Suhonen, A.; Mattila, M.; Leppaniemi, T.; Seppa, J. H.; et al. Contactless Electrical Sintering of Ag Nanoparticles on Flexible Substrates. *IEEE Trans. Microwave Theory Tech.* **2011**, *59*, 1419−1429.

(9) Simo, A.; Polte, J.; Pfander, N.; Vainio, U.; Emmerling, F.; Rademann, K. Formation mechanism of silver nanoparticles stabilized in glassy matrices. *J. Am. Chem. Soc.* **2012**, *134*, 18824−18833.

(10) Keirbeg, U.; Vollmer, M. *Optical Properties of Metal Clusters*; Springer, New York, 1995; Vol. *25*.

(11) Ju, S.; et al. Fabrication and optical characteristics of a novel optical fiber doped with the Au nanoparticles. *J. Nanosci. Nanotechnol.* **2006**, *6*, 3555−3558.

(12) Kelly, K. L.; Coronado, E.; Zhao, L. L.; Schatz, G. C. The Optical Properties of Metal Nanoparticles: The Influence of Size, Shape, and Dielectric Environment. *J. Phys. Chem. B* **2003**, *107*, 668−677.

(13) Battaglin, G.; et al. Z-scan study on the nonlinear refractive index of copper nanocluster composite silica glass. *Appl. Phys. Lett.* **2001**, *78*, 3953.

(14) Philip, R.; Kumar, G.; Sandhyarani, R. N.; et al. Picosecond optical nonlinearity in monolayer protected gold, silver, and gold-silver alloy nanoclusters. *Phys. Rev. B* **2000**, *62*, 13160.

(15) Chun, Y. X.; et al. Optical nonlinearity and ultrafast dynamics of ion exchanged silver nanoparticles embedded in sodalime silicate glass. *Chin. Bull. Sci.* **2008**, *53*, 695−699.

(16) Dong, Z.; et al. Annealing effect on the ultrafast dynamics of Ag nanoparticles embedded in soda-lime silicate glasses. *Phys. B* **2009**, *404*, 2122−2125.

(17) Nanda, K. K.; Sahu, S. N.; Benera, S. N. Liquid-drop model for the size-dependent melting of low-dimensional systems. *Phys. Rev. A* **2002**, *66*, No. 013208.

(18) Safaei, A.; Shandiz, M. A.; Sanjabi, S.; Barber, Z. H. Modelling the size effect on the melting temperature of nanoparticles, nanowires and nanofilms. *J. Phys.: Condens. Matter* **2007**, *19*, No. 216216.

(19) Koga, N.; Goshi, Y.; Yamada, S.; Pèrez-Maqueda, L. A. J. Kinetic Approach to Partially Overlapped Thermal Decomposition Processes. *J. Therm. Anal. Calorim.* **2013**, *111*, 1463−1474.

(20) Logvinenko; Polunina, V.; Mikhailov, O.; Mikhailov, Y.; Bokhonov, K. Study of Thermal Decomposition of Silver Acetate. *J. Therm. Anal. Calorim.* **2007**, *90*, 813−816.

(21) Wang, B. X.; Zhou, L. P.; Peng, X. F. Surface and Size Effects on the Specific Heat Capacity of Nanoparticles. *Int. J. Thermophys.* **2006**, *27*, 139.

(22) Galwey, A. K. Structure and Order in Thermal Dehydrations of Crystalline Solids. *Thermochim. Acta* **2000**, *355*, 181−238.

(23) Koga, N.; Tanaka, H. A Physico-Geometric Approach to the Kinetics of Solid-State Reactions as Exemplified by the Thermal Dehydration and Decomposition of Inorganic Solids. *Thermochim. Acta* **2002**, *388*, 41−61.

(24) Dong, Z.; Yang, X.; Li, Z.; You, G.; Yan, Y.; Quan, S. Annealing effect on the ultrafast dynamics of Ag nanoparticles embedded in soda-lime silicate glasses. *Phys. B* **2009**, *404*, 2122−2125.

(25) Kumar, M.; et al. Plasmonic and Nonlinear Optical Absorption Properties of Ag:ZrO_2 Nanocomposite Thin Films. *Plasmonics* **2014**, *9*, 129−136.

(26) De la Parra-Arciniega, S. M.; Alvarez-M endez, A.; Torres-Gonz alez, L. C.; Sanchez, E. M. Crystallization kinetics of a soda lime silica glass with TiO_2 addition. *Rev. Mex. Fis.* **2009**, *55*, 32−37.

(27) Hamanaka, Y. A.; et al. Dispersion curves of complex third-order optical susceptibilities around the surface plasmon resonance in Ag nanocrystal−glass composites. *J. Opt. Soc. Am. B* **2003**, *20*, 1227−1232.

(28) Villegas, M. A.; García, M. A.; Llopis, J. J.; Fernández Navarro, M. Optical Spectroscopy of Hybrid Sol-Gel Coatings Doped with Noble Metals. *J. Sol−Gel Sci. Technol.* **1998**, *11*, 251.

(29) Tan, N. P. B.; Lee, C. H.; Li, P. Green Synthesis of Smart Metal/Polymer Nanocomposite Particles and Their Tuneable Catalytic Activities. *Polymers* **2016**, *8*, 105.

(30) Mosquera, A. A.; Albella, J. M.; Navarro, V.; Bhattacharyya, D.; Endrino, J. L. Effect of silver on the phase transition and wettability of titanium oxide films. *Sci. Rep.* **2016**, *6*, No. 3217.

(31) Karunakaran, C.; Anilkumar, P.; Gomathisankar, P. Photoproduction of iodine with nanoparticulate semiconductors and insulators. *Chem. Cent. J.* **2011**, *5*, 31.

(32) Li, L. X.; Xu, D.; Li, X. Q.; Liuc, W. C.; de, Y. J. Excellent fluoride removal properties of porous hollow MgO microspheres. *New J. Chem.* **2014**, *38*, 5445−5452.

(33) Divakaran, S. A.; Sreekanth, K. M.; Rao, K. V.; Nair, C. K. D-Aminoacid Oxidase-Fe_2O_3 Nanoparticle Complex Mediated Antitumor Activity in Swiss Albino Mice. *J. Cancer Ther.* **2011**, *02*, 666.

(34) Wagner, C. D.; Riggs, W. M.; Davis, L. E.; Moulder, J. F.; Muilenberg, G. E. *Handbook of X-ray Photoelectron Spectroscopy*; Perkin-Elmer Corporation, Physical Electronics Division: Minnesota, 1979; p 190.

(35) Han, Z.; Zhang, J.; Yu, Y.; Cao, W. A new anode material of silver photo-deposition on TiO_2 in DSSC. *Mater. Lett.* **2012**, *70*, 193−196.

(36) García, M. A.; et al. Photoluminescence of silver in glassy matrices. *J. Appl. Phys.* **2004**, *96*, 3737−3741.

(37) Ferraris, M.; et al. Effect of thermal treatments on sputtered silver nanocluster/silica composite coatings on soda-lime glasses: ionic exchange and antibacterial activity. *J. Nanopart. Res.* **2012**, *14*, 1287−1306.

DOI: 10.1021/acsomega.7b00672
ACS Omega 2017, 2, 5748−5758

(38) Durucan, C.; Akkopru, B. Effect of Calcination on Microstructure and Antibacterial Activity of Silver-Containing Silica Coatings Caner. *J. Biomed. Mater. Res., Part B* **2010**, *93*, 448−458.
(39) Araujo, R. Colorless glasses containing ion-exchanged silver. *Appl. Opt.* **1992**, *31*, 5221−5224.
(40) Sheng, J.; Wu, Y.; Yang, X.; Zhang, J. Formation and optical properties of copper nanoclusters in a silicate glass. *Int. J. Hydrogen Energy* **2009**, *34*, 1123−1125.
(41) Doremus, R. H. Optical Properties of Small Silver Particles. *J. Chem. Phys.* **1965**, *42*, 414.
(42) Qi, W. Nanoscopic Thermodynamics. *Acc. Chem. Res.* **2016**, *49*, 1587−1595.
(43) Lai, S. L.; Guo, J.; Petrova, V.; Ramanath, G.; Allen, L. Size-Dependent Melting Properties of Small Tin Particles: Nanocalorimetric Measurements. *Phys. Rev. Lett.* **1996**, *77*, 99.
(44) Meloun, M.; Ferencíkova, Z. *Fluid Phase Equilib.* **2012**, *328*, 31−41.
(45) *CRC Handbook of Chemistry and Physics*; Weast, R. C.; Astle, M. J., Eds.; CRC Press: Boca Raton, FL, 1981; p F−216.
(46) Kistler, S. S. Stresses in Glass Produced by Nonuniform Exchange of Monovalent Ions. *J. Am. Ceram. Soc.* **1962**, *45*, 59−68.
(47) Kumar, P.; Mathpal, M. C.; Tripathi, A. K.; Prakash, J.; Agarwal, A.; Ahmad, M. M.; Swart, H. C. Plasmonic resonance of Ag nanoclusters diffused in soda-lime glasses. *Phys. Chem. Chem. Phys.* **2015**, *17*, 8596−8603.
(48) Lide, D. R., Ed.; *CRC Handbook of Chemistry and Physics*; CRC Press: Boca Raton, 1991; Vol. *5*−*38*, pp 5−49.

DOI: 10.1021/acsomega.7b00672
ACS Omega 2017, 2, 5748−5758